Aalborg Universitet

AALBORG UNIVERSITY
DENMARK

Measurement-based Feasibility Exploration on Detecting and Localizing Multiple Humans Using MIMO Radio Channel Properties

Miao, Yang; Tanghe, Emmeric; Takada, Jun-ichi; Pedersen, Troels; Laly, P.; Galliot, D.P.; Lienard, M.; Martens, L.; Joseph, Wout

Link to publication from Aalborg University

Measurement-Based Feasibility Exploration on Detecting and Localizing Multiple Humans Using MIMO Radio Channel Properties

YANG MIAO [1], **EMMERIC TANGHE** [2], **JUN-ICHI TAKADA** [3], **(Senior Member, IEEE),**
TROELS PEDERSEN [4], **PIERRE LALY** [5], **DAVY P. GAILLOT** [5], **MARTINE LIÉNARD** [5],
LUC MARTENS [2], **AND WOUT JOSEPH** [2],**(Member, IEEE)**

[1]Radio System Research Group, Telecommunication Engineering, Faculty of Electrical Engineering, Mathematics and Computer Science, University of Twente, 7522 NB Enschede, The Netherlands
[2]Ghent University–IMEC-WAVES, 9052 Gent, Belgium
[3]Department of Transdisciplinary Science and Engineering, Tokyo Institute of Technology, Tokyo 152-8552, Japan
[4]Department of Electronic Systems, Aalborg University, 9220 Aalborg East, Denmark
[5]Lille University–TELICE, 59655 Lille, France

Corresponding author: Yang Miao (yangmiao.career@outlook.com)

ABSTRACT This paper explores the feasibility of using the multiple-input multiple-output (MIMO) radio channel properties to passively detect and localize multiple humans in indoor environments. We propose to utilize the unique reverberation characteristics of indoor channels for the purpose of detecting, and the power angular delay profile (PADP) for localizing humans. On the one hand, the reverberation time corresponds with the decay rate of multipath in a closed or partially closed cavity, and varies with the change of the number of humans or the moving of humans relative to the antennas at link ends. On the other hand, the PADP is proposed to be calculated by the Multiple Signal Classification (MUSIC) super resolution algorithm with frequency smoothing preprocessing. The proposed approach is evaluated based on real-world MIMO radio channel measurements obtained from a meeting room. Measurements with and without the presence of humans have been conducted, where the maximum number of humans considered is four. Humans facing different directions, either in parallel or orthogonal to the direct line between the transmit and the receive antennas have been taken into account. In term of the detection feasibility, it is found that the change of the number of humans as well as the change of their facing/moving directions inside the partial reverberant region can be reflected on the change of the reverberation time estimated from the power delay profile of channel. In term of the localization feasibility, it is found that single human location can be well associated to the peak of the variation of the PADP during his/her movement, while multiple humans' movements result in obvious power variation in the very vicinity of some of them, and also in the vicinity of some background objects that is far from target humans.

INDEX TERMS Indoor radio channel, MIMO, reverberation time, power delay angular profile, passive detection and localization of humans.

I. INTRODUCTION

Device-free passive indoor localization plays a critical role for the emerging assisted-living applications [1], [2], such as the elder/child/disability care, smart home, etc. A device-free localization (DFL) system does not require human to wear or carry devices in order to be detected or localized. Radio-based

DFL systems are easily compatible with the existing wireless networks (e.g., Wi-Fi, cellular), and do not put constraints on the visibility conditions of the physical environment hence bring less concerns about privacy issues than camera- or visible light-based DFL systems where people are "watched" directly through image data or under visible conditions.

Typical techniques applied in radio-based DFL systems employ the time of arrival (ToA), the angle of arrival (AoA), the received signal strength (RSS), or the complex channel

The associate editor coordinating the review of this manuscript and approving it for publication was Luyu Zhao.

state information (CSI) [3]–[7]. In addition, fingerprinting [8], [9] or antenna array based DFL systems [10], [11] are also popular. Fingerprinting is mostly applied in RSS systems and consists of an offline phase to build a reference data base from surveyed signals at known positions. The offline phase is labor intensive and the approach is not robust against environmental changes. Also, a DFL system based on fingerprinting normally requires large number of sensor nodes/anchors to be deployed, and is difficult to apply if not compatibly designed with the target environment.

Alternatively, multiple input multiple output (MIMO) wireless radio systems become the feasible solution for DFL [12], and are easily available due to the current development of massive MIMO for next generation communication networks. The narrowband antenna arrays with spatial resolution can be used for measuring the spatial domain radio propagation characteristics, e.g., the information of AoA, the power angular profile. The MIMO DFL system does not require offline training, but the challenge is that the signals interacting with human bodies may be too weak and are buried among the undesired multipath interacting with background objects, especially for indoor scenarios with complex physical configurations. The presence and movement of humans in the propagation environment result in some paths being blocked or unblocked [3]. The changes in power spatial profile may not be linked to the actual location of the humans in a simple manner due to the multi-reflection or multi-scattering in particular for the real-world indoor environment with various background objects, and this fact makes the DFL using MIMO radio channel properties challenging.

Available MIMO radio channel based DFL algorithms rely on the "decent" resolution of a MIMO system in the spatial-temporal domains. The "decent" resolution can be achieved by a combination of 1) purely by system design with large bandwidth and/or large array aperture, and 2) the use of the super-resolution algorithms for multipath extraction from measurable channel transfer functions (or channel impulse response). Even though super-resolution algorithms can somewhat help, their accuracy is still limited when paths are close together, especially when the system bandwith or/and the spatial aperture size of antennas are not sufficiently large hence paths are not separated in delay or/and spatial domains. This is a fundamental limitation which also shows in, e.g., the Cramer-Rao bound on the estimation accuracy, and it is possible that super-resolution algorithms may introduce false multipath or false detected scatterer. In [13], an ultra-wide bandwidth (UWB) MIMO system has been used to successfully detect the remote breathing patterns of human for localization purpose, together with the use of the super-resolution RIMAX (iterative maximum-likelihood estimation scheme) algorithm for multipath extraction and linear antenna arrays at link ends. Reference [14], [15] have utilized the monostatic radar system and UWB transmissions for device-free localization. The transmit and receive antennas in a monostatic radar system are co-located, while they are separated in a certain distance in a bistatic radar system.

For the same power level, the monostatic radar systems have a much lower spatial range of operation than bistatic radar system [16], hence [14] needed distributed monostatic radars for the human detection purpose. Moreover, the perfect condition combining both the UWB MIMO system and the super-resolution algorithm on multipath extraction in [13] is not always available, [17], [18] demonstrated the localization of human through super-resolution algorithm in bistatic MIMO system without UWB. In [17], [18], the authors have utilized the bistatic MIMO radars and the MUSIC (MUltiple SIgnal Classification) algorithm on multipath extraction to estimate the human direction relative to the antenna locations. They also utilized the system's Doppler radar cross-section for estimating the posture of a human at dedicated location. The accuracy rate for localization and posture identification is reported to reach 90%, but the scenario is rather ideal where the person was located at the dedicated location that could surely produce reflections between link ends. In addition to the above mentioned work localizing one human, [19], [20] have been able to localize multiple humans (static but breathing, or moving) using MIMO radars with carrier frequencies across UWB.

However, to the best of our knowledge, there is not yet an investigation on localizing multiple humans using MIMO radio channels without a desired large bandwidth (larger than 500 MHz). Without investigating this, we will not know whether the lower system configuration (obviously with lower cost) can be used for multiple-human scenario. The intention of this work is to investigate if such non-UWB system can be used and explores the feasibility of detecting and localizing multiple humans (up to four) by using the indoor MIMO radio channel with a small bandwidth (less than 100 MHz). To this end, we propose to use the reverberation characteristic that is unique for indoor radio channel, as well as the power angular delay profile calculated by the modified MUSIC with the modified smoothing technique which has control over both the spatial sampling and the frequency sampling. The evaluation of the proposed approach in detecting and localizing humans is based on the MIMO radio channel measurement using the MIMOSA channel sounder [21] at 1.35 GHz with 80 MHz bandwidth, with dual-polarized planar patch antenna arrays at both link ends.

The rest of this paper is organized as follows. Section II reviews the MIMO radio channel properties and illustrates the proposed approach for detecting and localizing multiple humans. Section III describes the measurement campaign and the system parameters. Section IV provides numerical examples and evaluations. Section V concludes this paper. Throughout this paper, $(\cdot)^H$ indicates the conjugate transpose of the vector/matrix $(\cdot)$, $(\cdot)^T$ indicates the transpose, $(\cdot)^*$ indicates the conjugate, and $\otimes$ denotes the Kronecker product.

II. PROPOSED APPROACH
In this section, first, the MIMO radio channel properties in the temporal domain and in the joint spatial-temporal domains

are reviewed. Second, the proposed detection and localization scheme is introduced. For the spatial-temporal domain channel property, we propose to use the modified MUSIC with the modified smoothing pre-processing to optimally enlarge the accuracy of the estimate in spatial domain from the measurable radio channel. We do not claim that it is the only suitable super-resolution algorithm that can be used; there are other subspace based or maximum likelihood based algorithms, and the applicability is determined by whether there is considerable model mismatch to the measurement system [22]. The other reason to use the MUSIC based algorithm here is to be consistent hence be fair to compare with the work of localizing single human by using bistatic MIMO radars and MUSIC algorithm in [17], [18].

A. MIMO RADIO CHANNEL PROPERTIES

We denote the measurable channel transfer function (CTF) as $\boldsymbol{H}_{XY} \in \mathbb{C}^{N_R \times N_T}$:

$$\boldsymbol{H}_{XY}(f) = \begin{bmatrix} h_{XY,11}(f) & \cdots & h_{XY,1N_T}(f) \\ \vdots & \ddots & \vdots \\ h_{XY,N_R1}(f) & \cdots & h_{XY,N_RN_T}(f) \end{bmatrix}, \quad (1)$$

where h_{XY,n_rn_t} at each sampling frequency f is the element of matrix $\boldsymbol{H}_{XY}(f)$, $XY \in \{VV, VH, HV, HH\}$ indicates the polarized pair of antennas, V indicates vertical polarization, H indicates horizontal polarization. N_R and N_T are the total numbers of the receive (Rx) and the transmit (Tx) array antennas, respectively. $n_r = 1, 2, \ldots, N_R$ and $n_t = 1, 2, \ldots, N_T$ are the indices of Rx and Tx antennas, respectively. The inverse Fourier transform of CTF is called the channel impulse response (CIR).

1) TEMPORAL DOMAIN CHANNEL PROPERTY

The time domain channel is characterized by the power delay profile (PDP) given by

$$\text{PDP}(\tau) = \frac{1}{N_R N_T}$$
$$\times \sum_{XY} \sum_{n_r=1}^{N_R} \sum_{n_t=1}^{N_T} \left| \text{IFFT}\left\{\text{HannWindow}\left\{h_{XY,n_rn_t}(f)\right\}\right\}\right|^2,$$
$$(2)$$

where the Hann window is multiplied with CTF to suppress side-lobes, before the inverse Fourier transform is used to convert frequency signals to delay (denoted by τ) domain signals.

For indoor radio channels, an exponential slope in the "tail" of PDP can be expected [23]–[26], as demonstrated in Figure 1. The exponential slope normally stems from the reverberant components, e.g., the multiple reflections/scatterings, in a closed or partially closed environment. From the exponential slope that represents the decay rate of reverberant multipath, the reverberation time [24], denoted as T_{rev}, can be further estimated:

$$T_{rev} = -\frac{10}{\ln(10)\,slope} \approx -\frac{4.34}{slope}, \quad (3)$$
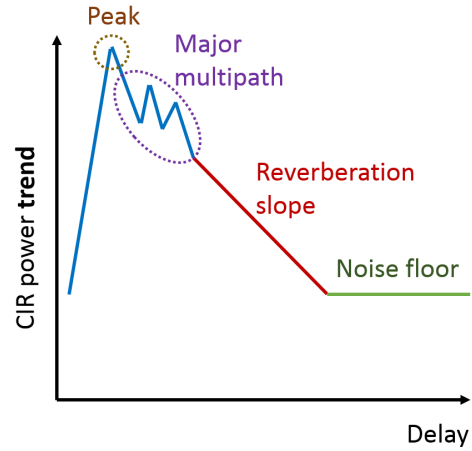

FIGURE 1. Schematic diagram of the PDP in typical indoor radio channel.

where *slope* has the unit of dB per second. Observation domain with fixed delay or power range can be applied to the PDP to calculate T_{rev}, and typically the range is visually determined by taking into account the effects of noise floor [23], [25]–[28].

On the other hand, as discussed in [23], the reverberation time can be modeled empirically using the Sabine's model [29]

$$T_{rev} = \frac{4V}{Sc\bar{a}} \quad (4)$$

or the Eyring's model [30]

$$T_{rev} = -\frac{4V}{Sc\ln(1-\bar{a})}, \quad (5)$$

where V is the volume of the indoor environment, S is the total surface area that absorbs radio waves, c is the speed of light, and $\bar{a}$ is the area weighted average absorption coefficient of all objects in the physical environment. Sabine's model is the first order Taylor expansion of the Eyring's model, and is most suited for situations with relatively low absorption, i.e. very reverberant cases. In most indoor radio propagation environments, however, are relatively "dead" in terms of reverberation and hence Eyring's model is most accurate [24]. Note that Eyring's model in (5) can be further improved by applying the Kuttruff correction factor, as has been shown in [31]. In both of these models, reverberation time is a function of the average absorption coefficient, the volume, and the surface area specific to the considered indoor environment.

With the increase or the decrease of the number of presenting humans, or with the moving of humans relative to the Tx/Rx antennas, the power absorbed by humans varies, leading to a change in average absorption coefficient and absorption area hence a change in the value of T_{rev}. Note that the influence of humans on reverberation time depends on many factors, such as the body surface area, the body component (fat or muscle), the clothes worn, the posture and the facing direction to antennas and the antenna radiation

patterns, etc., [32]. In addition, the exposed surface area differs in case the person is standing, sitting or lying down, with the latter yielding the minimum absorption area.

2) SPATIAL-TEMPORAL DOMAIN CHANNEL PROPERTY

The spatial domain channel can be characterized jointly with the temporal domain by the power angular delay profile (PADP), which holds geometrical information on the scatterers interacting with radio waves.

We propose to use the modified MUSIC super resolution algorithm, to be consistent with the existing work using non-UWB bistatic MIMO radars in [17], [18] as mentioned previously. In addition, we use the modified smoothing pre-processing to achieve a better accuracy in classifying paths, where we sacrifice the frequency samplings for decorrelation purpose hence an improved observation in spatial domain. According to [33], weak signals are combined if the number of signals is underestimated. To tackle that, super resolution algorithm performs well even in severe multipath environments as the under-determined solution, and the overestimation of dimension of signal subspace preserves the estimates of typical signals. The frequency smoothing preprocessing [34] is applied to decorrelate the coherent measured signals. The decorrelation by frequency smoothing depends on the time difference of the waves and the frequency distance of the samples [34], [35]. The correlation of signals with very short time difference (''continuous'' PDP for instance) will not be sufficiently decorrelated on the narrowband measurement. In addition, smoothing among frequency samples, rather than among spatial samples, is preferred here for two reasons: 1) the frequency domain sampling size can be set much larger than the spatial domain sampling size which is determined by the number of array antennas; 2) giving up frequency points in the observation domain harms less the estimation resolution than giving up spatial points because localization is based on spatial information from the PADP.

Referring to [7], [33]–[36], we modify the MUSIC spectrum to involve as much spatial-temporal information as possible from the given system configuration, and the spectrum is given by

$$
\begin{aligned}
&P_{\mathrm{MUS}} \left(\phi_{\mathrm{R}}, \theta_{\mathrm{R}}, \phi_{\mathrm{T}}, \theta_{\mathrm{T}}, \tau \right) \\
&= \sum_{XY} \frac{\boldsymbol{B}^H \left(\phi_{\mathrm{R}}, \theta_{\mathrm{R}}, \phi_{\mathrm{T}}, \theta_{\mathrm{T}}, \tau \right) \boldsymbol{B} \left(\phi_{\mathrm{R}}, \theta_{\mathrm{R}}, \phi_{\mathrm{T}}, \theta_{\mathrm{T}}, \tau \right)}{\boldsymbol{B}^H(\phi_{\mathrm{R}}, \theta_{\mathrm{R}}, \phi_{\mathrm{T}}, \theta_{\mathrm{T}}, \tau) \boldsymbol{E}_{\mathrm{N},XY} \boldsymbol{E}_{\mathrm{N},XY}^H \boldsymbol{B}(\phi_{\mathrm{R}}, \theta_{\mathrm{R}}, \phi_{\mathrm{T}}, \theta_{\mathrm{T}}, \tau)},
\end{aligned}
\tag{6}
$$

and

$$
\begin{aligned}
&\boldsymbol{B} \left(\phi_{\mathrm{R}}, \theta_{\mathrm{R}}, \phi_{\mathrm{T}}, \theta_{\mathrm{T}}, \tau \right) \\
&= \boldsymbol{A}_{\mathrm{T}} \left(\phi_{\mathrm{T}}, \theta_{\mathrm{T}} \right) \otimes \boldsymbol{A}_{\mathrm{R}} \left(\phi_{\mathrm{R}}, \theta_{\mathrm{R}} \right) \otimes \boldsymbol{b} \left(\tau \right) \quad \in \mathbb{C}^{(N_f N_{\mathrm{R}} N_{\mathrm{T}}) \times 1},
\end{aligned}
\tag{7}
$$

where $\boldsymbol{B}$ is the steering vector involving both the phase differences among antenna elements in spatial domain and the phase differences among subcarriers after frequency

smoothing. The Tx steering vector is defined as

$$
\begin{aligned}
&\boldsymbol{A}_{\mathrm{T}} \left(\phi_{\mathrm{T}}, \theta_{\mathrm{T}} \right) \\
&= [a_{\mathrm{T},1} \left(\phi_{\mathrm{T}}, \theta_{\mathrm{T}} \right), \cdots, a_{\mathrm{T},N_{\mathrm{T}}} \left(\phi_{\mathrm{T}}, \theta_{\mathrm{T}} \right)]^T \in \mathbb{C}^{N_{\mathrm{T}} \times 1}
\end{aligned}
\tag{8}
$$

with

$$
a_{\mathrm{T},n_{\mathrm{t}}} \left(\phi_{\mathrm{T}}, \theta_{\mathrm{T}} \right) = \exp \left(-j \frac{2\pi}{\lambda} \left(\hat{\boldsymbol{k}}_{\mathrm{T}} \cdot \bar{\boldsymbol{r}}_{\mathrm{T},n_{\mathrm{t}}} \right) \right),
\tag{9}
$$

where λ is the wavelength, and $\hat{\boldsymbol{k}}_{\mathrm{T}}$ is a unit vector in the direction $(\phi_{\mathrm{T}}, \theta_{\mathrm{T}})$, i.e.

$$
\hat{\boldsymbol{k}}_{\mathrm{T}} = [\sin (\theta_{\mathrm{T}}) \cos (\phi_{\mathrm{T}}), \sin (\theta_{\mathrm{T}}) \sin (\phi_{\mathrm{T}}), \cos (\theta_{\mathrm{T}})].
\tag{10}
$$

The vector $\bar{\boldsymbol{r}}_{\mathrm{T},n_{\mathrm{t}}}$ gives the position of n_{t}-th element of Tx array in local coordinate. The array vector for the Rx is similarly defined by swapping subscripts r and R for t and T. The azimuth and co-elevation angles of departure are denoted by ϕ_{T} and θ_{T}, respectively. Similarly the azimuth and co-elevation angles of arrival are denoted by ϕ_{R} and θ_{R}, respectively. The steering vector of the phase difference across subcarriers is

$$
\boldsymbol{b} \left(\tau \right) = \left[\Omega_1 \left(\tau \right), \ldots, \Omega_{N_f} \left(\tau \right) \right]^T \in \mathbb{C}^{N_f \times 1},
\tag{11}
$$

where

$$
\Omega_{n_f} \left(\tau \right) = \exp \left(-j2\pi f_\delta (n_f - 1)\tau \right),
\tag{12}
$$

f_δ is the subcarrier separation. Different paths have different times of arrival, the time differences may introduce measurable phase difference across subcarriers. The eigenvectors gathered in the matrix $\boldsymbol{E}_{\mathrm{N},XY} \in \mathbb{C}^{(N_f N_{\mathrm{R}} N_{\mathrm{T}}) \times (N_f N_{\mathrm{R}} N_{\mathrm{T}} - N_{\mathrm{s}})}$ correspond to the noise subspace spanned by the covariance matrix of $\boldsymbol{h}_{XY} \in \mathbb{C}^{N_f N_{\mathrm{R}} N_{\mathrm{T}} \times 1}$ which is composed by $h_{XY,n_{\mathrm{r}} n_{\mathrm{t}}}^{n_f}$, and N_{s} denotes the number of significant signals. Here the elements in $\boldsymbol{E}_{\mathrm{N},XY}$ are determined according to the insignificant eigenvalues [37]. The significant eigenvalues used in this paper are determined with a 95% confidence level in the cumulative distribution. The modified smoothing technique in [34] is applied before calculating the MUSIC spectrum. In the smoothing process, the correlation matrix of $\boldsymbol{h}_{XY}$ is defined by

$$
\begin{aligned}
\boldsymbol{R}_{\boldsymbol{h}_{XY}} = &\frac{1}{2 \left(N_{f0} - N_f + 1 \right)} \sum_{i=1}^{N_{f0} - N_f + 1} \left(\boldsymbol{h}_{XY}^i \boldsymbol{h}_{XY}^{i}{}^H \right. \\
&+ \left. \boldsymbol{J} \left(\boldsymbol{h}_{XY}^i \boldsymbol{h}_{XY}^{i}{}^H \right)^* \boldsymbol{J} \right) \in \mathbb{C}^{N_f N_{\mathrm{R}} N_{\mathrm{T}} \times N_f N_{\mathrm{R}} N_{\mathrm{T}}},
\end{aligned}
\tag{13}
$$

where N_{f0} and N_f are the numbers of subcarriers before and after frequency smoothing preprocessing, respectively. $N_{f0} - N_f + 1$ indicates the number of frequency subarrays after smoothing, and i is the index for the subarrays. The exchange matrix is denoted as $\boldsymbol{J} \in \mathbb{C}^{N_f N_{\mathrm{R}} N_{\mathrm{T}} \times N_f N_{\mathrm{R}} N_{\mathrm{T}}}$, and the term $\boldsymbol{J} \left(\boldsymbol{h}_{XY} \boldsymbol{h}_{XY}^H \right)^* \boldsymbol{J}$ is added in the modified smoothing technique to enhance the effect of destroying the signal coherence. Eigen decomposition of $\boldsymbol{R}_{\boldsymbol{h}_{XY}}$ results in an eigenvector $\boldsymbol{E}_{XY}$ and diagonal matrix $\boldsymbol{V}_{XY}$ whose diagonal elements are the corresponding eigenvalues.

B. PROPOSED DETECTION AND LOCALIZATION SCHEME, AND MEASUREMENT TECHNIQUE

We propose a method for detecting and localizing multiple humans by the use of a MIMO system without large bandwidth (narrower than 100 MHz). We aim at exploiting the most of the spatial information from the measurable non-UWB MIMO CTF to localize moving humans, that is, 1) the move from one location to another (denoted as MOV1), and 2) the move to turn to different direction but stay at the same location (denoted as MOV2).

During the measurement, at each time, several snapshots (time duration denoted as t_{sp}) of CTF or CIR are measured at entire frequency points to ensure the reliability of data and to minimize the effect of noise. The CTF or CIR is measured periodically at time interval t_{it}, and we compare the MIMO channel properties measured at t and that at $t + t_{it}$ (i.e. at every t_{it}) in terms of PDP, reverberation time T_{rev}, and PADP. Here we define the reverberation time variation $\Delta T_{rev}|_t^{t+t_{it}}$ as:

$$\Delta T_{rev}|_t^{t+t_{it}} = \left| T_{rev,t} - T_{rev,t+t_{it}} \right|, \qquad (14)$$

the PDP variation $\Delta PDP(\tau)|_t^{t+t_{it}}$ as:

$$\Delta PDP(\tau)|_t^{t+t_{it}} = \left| PDP_t(\tau) - PDP_{t+t_{it}}(\tau) \right|, \qquad (15)$$

and the PADP variation $\Delta P_{MUS}(\phi_R, \phi_T, \tau)|_t^{t+t_{it}}$ as:

$$\Delta P_{MUS}(\phi_R, \phi_T, \tau)|_t^{t+t_{it}} = \left| P_{MUS,t}(\phi_R, \frac{\pi}{2}, \phi_T, \frac{\pi}{2}, \tau) \right.$$
$$\left. - P_{MUS,t+t_{it}}(\phi_R, \frac{\pi}{2}, \phi_T, \frac{\pi}{2}, \tau) \right|. \qquad (16)$$

Here, for the purpose of localization, we are more interested in the azimuth domain. Therefore, the five dimensional parameter estimation in (6) is simplified to the three dimensional parameter estimation of ϕ_T, ϕ_R, τ by setting θ_T and θ_R as $\frac{\pi}{2}$, as in (16). With the comparison between T_{rev} at adjacent channel samplings, and the comparison between the modified MUSIC spectrum (with well controlled degree-of-freedom on exploiting the super resolution) at adjacent channel samplings, the detection and the localization of multiple humans can be achieved at certain accuracy.

In this paper, the part of PDP considered for estimating the T_{rev} starts from the delay bin with power 20 dB lower than the peak power, ends at the delay with power 3 dB above the noise floor. The noise floor is defined the same way as in [27]. The numerical analysis will be illustrated in Section IV.

III. MEASUREMENT CAMPAIGN

Radio channel measurements were performed with the MIMOSA channel sounder [21]. The settings of the sounder are given in Table 1. The sounder supports 8 transmitting and 16 receiving parallel channels. Orthogonal frequency division multiplexing (OFDM) is used to encode the digital transmit symbols, dividing the 80 MHz bandwidth into 6560 sub-carriers equally split among 8 parallel transmit channels. This yields an inter-frequency spacing of 12.2 kHz

TABLE 1. MIMOSA channel sounder parameters.

Center frequency f_c	1.35 GHz
Bandwidth BW	80 MHz
Number of OFDM sub-carriers	6560
OFDM symbol duration T_S	81.92 μs
Cyclic prefix duration T_{CP}	40 μs
Number of transmit channels	8 parallel (16 in switch)
Number of receive channels	16 parallel
16×16 channel acquisition time	295.04 μs = $51.2 + 2 \times (T_S + T_{CP})$ μs

and an OFDM symbol duration is about 82 μs. The cyclic prefix is chosen to be a fraction of the symbol duration. Each transmit channel is connected to a two-state RF switch, therefore 16×16 channels can be measured and it costs at most 295.04 μs for one snapshot. Both link ends are equipped with planar arrays with each 8 dual-polarized patch antennas. The array element spacing and positions of element center are shown in Table 2. In addition, as shown in Figure 2, arrays are placed vertically parallel to the wall.

TABLE 2. Patch array placement, given in carrier wavelengths $0.5\lambda_c$, where $\lambda_c = \frac{c}{f_c}$ is the wavelength at central frequency f_c.

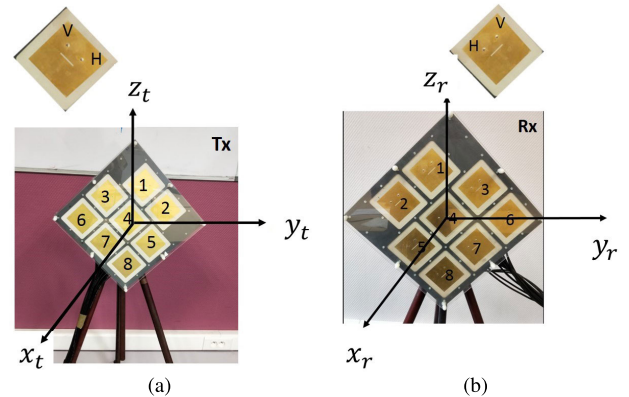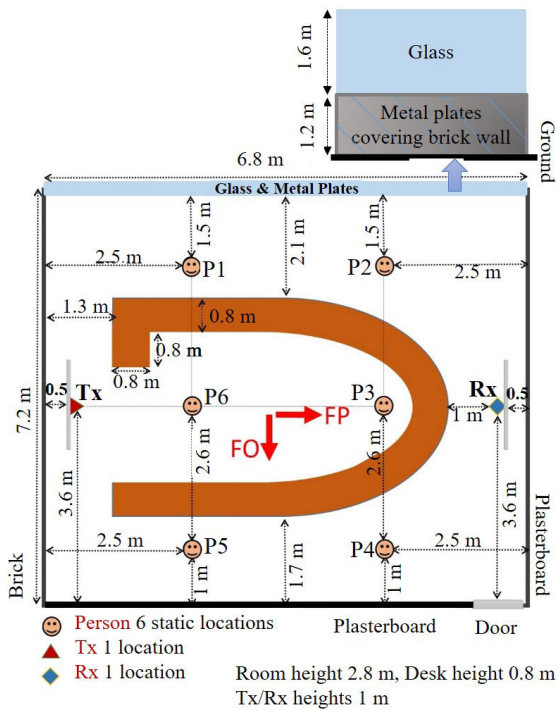| Index	Tx position	Rx position
1	(0, 0.35, 1.06)	(0, −0.35, 1.06)
2	(0, 1.06, 0.35)	(0, −1.06, 0.35)
3	(0, −0.71, 0.71)	(0, 0.71, 0.71)
4	(0, 0, 0)	(0, 0, 0)
5	(0, 0.71, −0.71)	(0, −0.71, −0.71)
6	(0, −1.41, 0)	(0, 1.41, 0)
7	(0, −0.71, −0.71)	(0, 0.71, −0.71)
8	(0, 0, −1.41)	(0, 0, −1.41)

FIGURE 2. Dual-polarized patch antenna array (a) Tx patch array (b) Rx patch array, where θ and ϕ are the co-elevation and azimuth angles.

The measurements were conducted in a meeting room in Lille University, France. Figure 3 shows the floor plan with Tx and Rx locations. The floor and ceiling are made of concrete, the outer wall (top side in Figure 3) consists of windows and concrete structures, while the inner walls are plasterboard. In addition, there are meeting tables and chairs. The door was open during the measurement and the windows were kept shut. Both arrays were set to fixed locations.

FIGURE 3. Floor plan with Tx, Rx, person locations (P1 - P6, where P1, P2, P4, P5 are outside of the first Fresnel zone of Tx and Rx, and P3, P6 are inside), FP indicates Facing in Parallel, FO indicates Facing in Orthogonal to the direct line between Tx and Rx.

TABLE 3. Reverberation time calculated from PDP.

Number of person in room	inside 1st Fresnel zone	Person @ location	Reverberation time [ns] FO	FP
1	0	Y@P1	45.6	46.4
		E@P1	45.5	46.4
		Y@P2	44.6	45.8
		E@P2	45.2	45.7
		Y@P4	44.2	45.2
		E@P4	45.5	45.5
		Y@P5	45.3	44.8
		E@P5	44.8	45.0
	1	Y@P3	39.2	38.2
		E@P3	38.0	37.5
		Y@P6	39.4	40.5
		E@P6	39.1	37.6
2	0	Y@P1,E@P2	45.6	45.9
		Y@P1,E@P4	45.4	45.3
		Y@P1,E@P5	45.0	46.3
		Y@P2,E@P1	44.9	46.0
		Y@P2,E@P4	44.9	45.2
		Y@P2,E@P5	43.4	45.1
		Y@P4,E@P1	44.4	45.7
		Y@P4,E@P2	45.7	45.5
		Y@P4,E@P5	45.1	45.0
		Y@P5,E@P1	44.9	46.2
		Y@P5,E@P2	44.2	45.2
		Y@P5,E@P4	45.4	45.4
	1	Y@P1,E@P3	37.9	34.0
		Y@P1,E@P6	39.6	39.5
		Y@P2,E@P3	37.3	37.9
		Y@P2,E@P6	37.9	38.7
		Y@P3,E@P1	39.1	40.2
		Y@P3,E@P2	40.7	40.0
		Y@P3,E@P4	38.9	38.9
		Y@P3,E@P5	38.8	39.4
		Y@P4,E@P3	37.3	37.1
		Y@P4,E@P6	39.1	34.6
		Y@P5,E@P3	36.9	37.7
		Y@P5,E@P6	39.5	36.6
		Y@P6,E@P1	39.7	42.0
		Y@P6,E@P2	39.9	38.8
		Y@P6,E@P4	39.6	40.2
		Y@P6,E@P5	39.7	40.3
	2	Y@P3,E@P6	33.5	28.6
		Y@P6,E@P3	33.5	28.6
3	0	Y@P1, E@P5, F@P4	44.6	45.7
		Y@P5, E@P1, F@P2	45.9	44.7
	1	Y@P3, E@P4, F@P2	39.0	38.9
		Y@P6, E@P1, F@P2	40.2	41.3
		Y@P6, E@P5, F@P1	40.3	41.7
		Y@P6, E@P5, F@P4	39.4	41.0
	2	Y@P1, E@P6, F@P3	31.7	28.9
		Y@P5, E@P6, F@P3	32.2	30.6
4	0	Y@P5, E@P1, F@P2, N@P4	46.0	45.5
	1	Y@P6, E@P5, F@P4, N@P2	40.0	40.3
		Y@P5, E@P1, F@P2, N@P3	37.3	35.1
	2	Y@P5, E@P6, F@P3, N@P2	29.1	29.6
		Y@P3, E@P5, F@P4, N@P6	32.9	30.2
		Y@P3, E@P1, F@P2, N@P6	33.2	34.9
0				45.5

They were parallel to wall surfaces and radiated radio waves towards inside the room. Different from the measurement settings in [13], [17], [18], the measurement presented in this paper is the obstructed line-of-sight (O-LOS) scenario; the meeting table presented in the very first Fresnel zone between Tx/Rx as well as the side walls behind Tx/Rx result in the co-existence of the LOS, the reflected, and the multiple-reflected paths in the zone.

The channels were measured with and without humans, where the former considered up to four persons standing at six different locations and facing either in parallel (FP) or orthogonal (FO) to the direct line between Tx and Rx. The measurement scenarios are summarized in Table 3, where Y, E, F, N stand for four different persons. Each radio channel was measured 15 times (snapshots) assuming static conditions within 4.5 ms ($t_{sp} <= 15 \times 295.04 \ \mu s$). Outlier elimination [38] is implemented to exclude the snapshots with errors due to mechanical vibration or switching errors of the channel sounder. Such snapshots have significantly different powers from the rest and are usually rare. The good snapshots for one measurement are supposed to be perfectly correlated under reasonable signal-to-noise ratio.

With no humans present, the measured channel is a collection of the direct path and the paths interacting with background objects. With humans present, the measured channel contains not only the formerly mentioned paths but also paths interacting with the bodies; the changes in the number of humans, or position and gesture may influence the

background paths. We aim at localizing humans by identifying the changes in MIMO radio channel properties caused by the movement of humans: MOV1 and MOV2. We differentiate the spatial-temporal changes that are directly linked
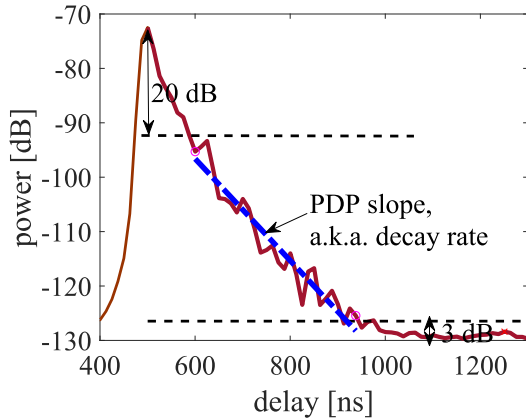
FIGURE 4. An example of calculating the PDP slope.

to the human by comparing the proposed channel properties in adjacent samplings of measured channel. The change in the number of humans is mimicked by comparing the measured channels without person and/or with different persons, the movement of humans can be mimicked by comparing the channels when humans face different directions or standing at different locations.

IV. DATA ANALYSIS

First, the feasibility of using the reverberation time calculated from PDP for the purpose of multiple-human detection is demonstrated. Second, the PADP calculated from the modified MUSIC spectrum with modified smoothing preprocessing is justified for its capability in localizing multiple humans.

A. PDP, REVERBERATION TIME, AND MULTI-HUMAN DETECTION

Figure 4 provides an example of the averaged PDP over snapshots as well as the fitted slope for the measured channel when person E stands at P1 in direction of FP. Consecutive multipath peaks appear in the observation domain on the slope. Through the linear fitting of the considered range, the slope rate is -0.094 dB/ns, hence the reverberation time is 46.4 ns. The same procedure is applied with fixed power range to all the measured scenarios. The resulting reverberation times are reported in Table 3, Figure 5 and Figure 6. Since we use the reverberation time as one important parameter to compare, we need to make sure the accuracy of the determined reverberation times by evaluating the confidence intervals. Notable observations from the data in Table 3, Figure 5 and Figure 6 are summarized as follows.

First, no matter how many people (maximum 4) are present in room, as long as the humans are not inside the 1st Fresnel zone of Tx and Rx, the reverberation time varies only little from the situation with no one in the room. Moreover, in this case, the reverberation time when human posing FO (mean 45.0 ns, standard deviation (std) 0.6 ns) and that when FP (mean 45.5 ns, std 0.5 ns) do not have significant differences either.

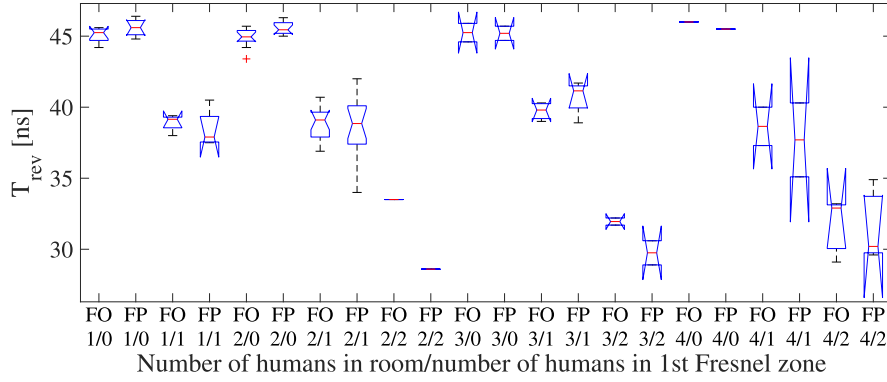**TABLE 4.** Statistics of reverberation time of measurement scenarios.

Wilcoxon rank sum test p value			Number of persons inside 1st Fresnel zone					
			0		1		2	
			FO	FP	FO	FP	FO	FP
Number of persons inside 1st Fresnel zone	0	FO	\	0.01	0	0	0	0
		FP		\	0	0	0	0
	1	FO			\	0.97	0	0
		FP				\	0	0
	2	FO					\	0.07
		FP						\
T_{rev} median [ns]			45.1	45.5	39.2	38.9	32.9	29.6

Second, no matter how many humans in total (maximum 4) in the room, the increase of one human inside the 1st Fresnel zone causes the decrease of about 5.9 ns to 6.6 ns in the reverberation time, and the increase of two humans inside the zone causes the decrease of about 12.2 ns to 15.9 ns. With more humans, the facing directions of them relative to the direct line between Tx and Rx influence more on the reverberation time, e.g. two humans with FO cause 12.2 ns decrease in T_{rev}, while two humans with FP cause 15.9 ns decrease.
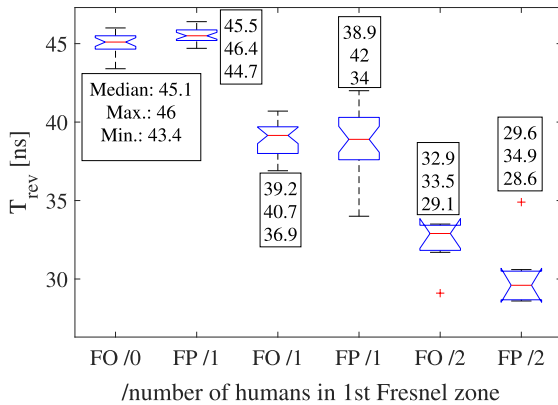
To analyze the similarity of T_{rev} between FO and FP cases, the Wilcoxon rank sum test is conducted. The results are reported in Figure 6 and Table 4. The Wilcoxon rank sum test compares the hypothesis that two data sets are from continuous distributions with equal medians against the alternative that they are not. At the 5% significance level, the scenario with *one* person inside the Fresnel zone facing in direction of FO has a statistically equal median with that when FP, and the scenario with *two* persons inside the Fresnel zone facing in direction of FO has statistically equal median with that when FP. For the other scenarios, the Wilcoxon rank sum tests reject the null hypothesis of equal medians of T_{rev}.

Comparing with [27], this is a drastic change of T_{rev} resulting from human entering or leaving the 1st Fresnel zone. One of the reasons is the deployment of Tx and Rx where the direct path is in perpendicular to the side walls (left and right walls in Figure 3). Not only the reflected paths through the meeting table arrive Rx in directions similar to the direction of LOS direct path, but also the multiple reflected paths (higher order reflections with longer propagation distance) interacting with the side walls arrive Rx in directions similar to the direct path. The multiple reflections/scatterings by side walls and meeting table contribute to the reverberant components of the channel, and the presence of humans in the 1st Fresnel zone obstructed not only the major multipath but also the reverberation paths, so that a drastic change in the reverberation time occurs. It is interesting that the 1st Fresnel zone in this measurement setting seems to form a partial reverberant space that is sensitive to the number of humans presenting inside. When more than one human presents inside the zone, the resulting reverberation time varies with the body cross section relative to the direction of the direct path. From this point of view, we see the feasibility of detecting humans and estimating the number of humans with similar deployment of link ends as in this measurement set-ups.
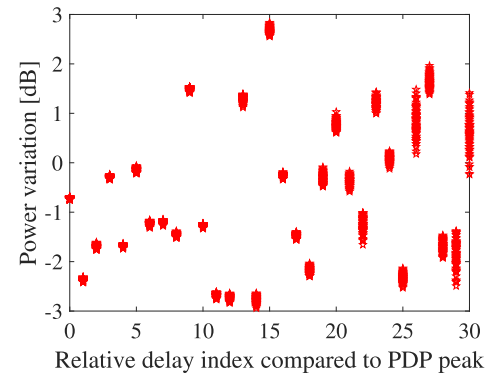
FIGURE 5. Mean and standard deviation (std) of T_{rev} for categorized measurement scenarios based on how many humans present in room, how many inside 1st Fresnel zone, and their facing direction.

FIGURE 6. Mean and std. of T_{rev} for categorized measurement scenarios based on how many inside 1st Fresnel zone and their facing direction.

FIGURE 7. Example of $\Delta PDP(\tau)|_t^{t+t_{it}}$, $\tau_{peak} \leq \tau \leq \tau_{tailend}$ for all snapshots, when no one is inside room at t, and Y (@P1), E (@P5), F (@P4) are inside room but outside of the 1st Fresnel zone at $t + t_{it}$, here relative delay index 0 denotes τ_{peak} and 30 corresponds to $\tau_{tailend}$.

On the other hand, the door was open to the corridor during the measurement; when multiple humans presenting in location P4 and P5, it seems that there is no obvious change in the reverberation time comparing to the case when no one inside the room. The same consequences on the reverberation time happen when multiple humans presenting in location P1 and P2 where the windows are nearby. The reason is the lack of the multiple reflections/scatterings arriving Rx from those regions outside of the 1st Fresnel zone, given the measurement setting. As explained in [23], the energy associated with the radio waves that are interacting with humans near the door or the windows may fled out of the room. It may also related to the fact that the number of humans is rather small in our measurement scenarios comparing to [27], and the reverberation time may have an obvious decrease if, say, 10 persons standing at around P5 even outside of the 1st Fresnel zone.

When the reverberation time variation $\Delta T_{rev}|_t^{t+t_{it}}$ is not obvious, alternatively, the PDP variation can be used to examine or detect the appearance or the disappearance of humans outside of the 1st Fresnel zone. The examination range can start from the peak of PDP (τ_{peak}) until the end of the PDP slope ($\tau_{tailend}$), i.e. $\Delta PDP(\tau)|_t^{t+t_{it}}$ for $\tau_{peak} \leq \tau \leq \tau_{tailend}$. If there are obvious (more than 2 dB) power variations in the examination range, we could suspect that the appearance

or the disappearance of humans or the movement of humans may happens outside of the 1st Fresnel zone. This suspect is based on the fact that the background objects have not been changed during the time intervals. Figure 7 shows an example and it can be observed that the maximum power change on target delay bins can reach 3 dB. This observation reminds us that the PDP variation will increase the feasibility of detection if both the reverberation time and PDP are compared between the channels measured at successive time intervals at t and $t + t_{it}$, although the detailed analysis on the PDP variation is out of the scope of this paper.

B. PADP AND MULTI-HUMAN LOCALIZATION

Here, the spatial-temporal channel property PADP is estimated by the method descried in Section II.A.2), and the PADP variations calculated from the observed channel at t and that at $t + t_{it}$ when humans are moving are used for localization purpose. We aim at localizing humans through their movements: MOV1 and MOV2. We assume that the humans' translational movement in space during the time interval of the observations on CTF is small enough so that the movement in category MOV1 can be described by the movement in category MOV2 but with several time intervals. As a result, we mainly focus on evaluating the capability of PADP

in multi-human localization when humans are in rotational movements at the same location; in our measurement setting, the rotational movements of humans are mimicked by from FO to FP or the contrary.

To reduce the cost of calculation time and memory on the available computers, the measured channel is downsized by smoothing it to obtain $N_{f_0} = 273$ frequency points uniformly sampled from 1.31 GHz to 1.39 GHz. During the frequency smoothing, the number of frequency subarray element N_f is set as 10, hence totally $N_{f_0} - N_f + 1 = 264$ frequency subarrays are used for the decorrelation of the signal space of measured channel. The delay resolution after smoothing is $\tau = 0.38\ \mu$s corresponding to the bandwidth of subarray of 2.65 MHz. Since the observation on frequency domain is sacrificed for the observation on spatial domain, the main PADP variations may be concentrated in the earlier one or two delay bins from the peak delay bin. In addition, the angular resolutions of ϕ_T and ϕ_R in (6) are set to 5°.
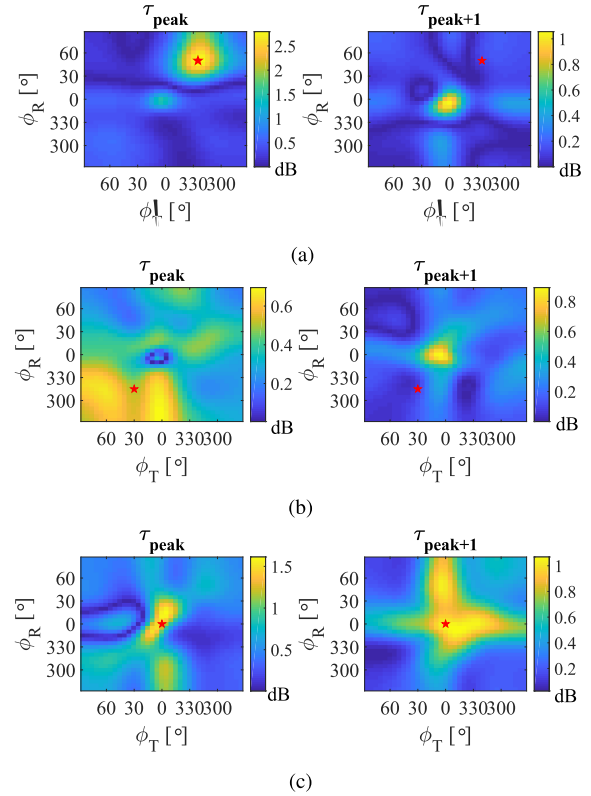
1) SINGLE HUMAN

Figure 8 (a) provides an example for person E standing at P4 and moving from FO to FP from t to $t + t_{it}$, or the other way around. We compare the PADP of the two channels measured at t and $t + t_{it}$, and plot the absolute difference. The sub-figures show $\Delta P_{MUS}(\phi_R, \phi_T, \tau)|_t^{t+t_{it}}$, at the peak delay bin τ_{peak} and the delay after the peak τ_{peak+1}. It can be observed that the peak of $\Delta P_{MUS}(\phi_R, \phi_T, \tau_{peak})|_t^{t+t_{it}}$ coincides with E's location P4, and the peak level of this variation is about 2.8 dB. At the following delay bin, no obvious connection between $\Delta P_{MUS}(\phi_R, \phi_T, \tau_{peak+1})|_t^{t+t_{it}}$ and E's location can be observed, but the 1 dB power variation in the 1st Fresnel zone of Tx and Rx seems to be caused by the human's movement. This variation could be owing to the multiple reflections/scatterings whose propagation paths interact with human and then the tables or/and the side walls.

Figure 8 (a) provides an example for localizing moving person standing at P4 that is at the door side, and Figure 8 (b) and (c) provide examples for one moving person at the window side P2 and in the Fresnel zone P3, respectively. It can be observed from both cases that the peak of $\Delta P_{MUS}(\phi_R, \phi_T, \tau_{peak})|_t^{t+t_{it}}$ is directly linked to the location of the human. From both Figure 8 (a) and (b), while the human stands outside of the 1st Fresnel zone, his movement causes power variations not only at his vicinity, but also inside the zone; the power variations inside the zone are due to the multiple reflections/scattering via firstly the human and later the physical objects inside the zone.

2) TWO HUMANS

Figure 9 shows several examples of the PADP variations of measured channels when two humans move from FP to FO (or the other way around) at the adjacent observation time. Figure 9 (a) and (b) show the examples when E stands and moves at P4, and Y stands and moves at the window
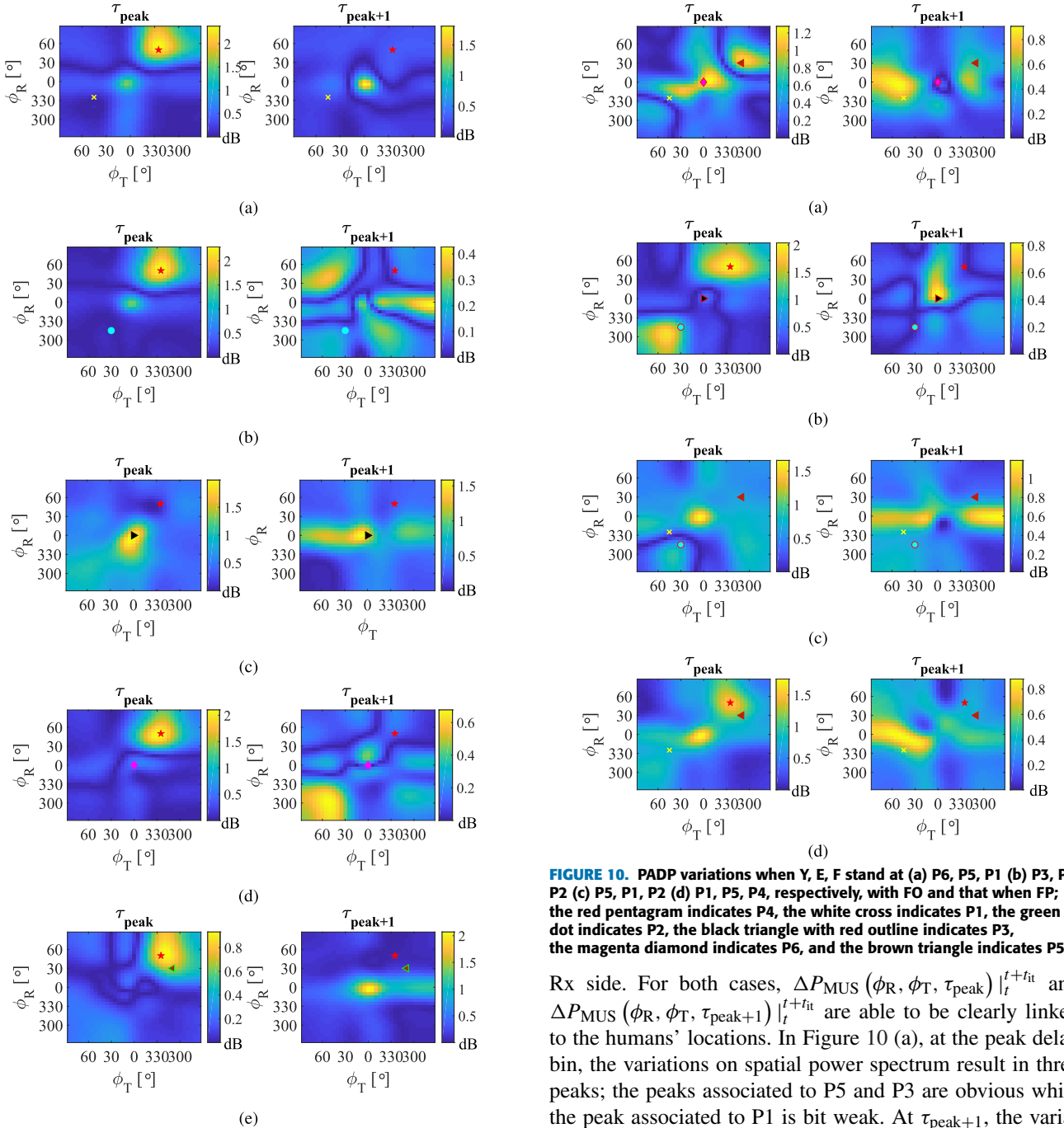

FIGURE 8. PADP variations when E stands at (a) P4 (b) P2 (c) P3 with FO and that when FP, the red pentagram indicates the actual location of E.

side. It can be observed that the peak of power variation $\Delta P_{MUS}(\phi_R, \phi_T, \tau_{peak})|_t^{t+t_{it}}$ can only be directly linked to P4, but the location of P1 and P2 can not be clearly indicated. It can be expected from Figure 8 (a) and (b) where the spatial power variation at τ_{peak} brought by person moving at P2 is about 2 dB smaller than that by person moving at P4. This poses the challenge of localizing multiple humans by only using the PADP variations.

Figure 9 (c) and (d) show the examples when E stands and moves at P4, and Y stands and moves inside the first Fresnel zone. When Y stands and moves at P3 which is closer to Rx, the peak of the spatial power variation $\Delta P_{MUS}(\phi_R, \phi_T, \tau_{peak})|_t^{t+t_{it}}$ clearly indicates the location of P3; when Y stands and moves at P6 which is closer to Tx, the peak of the spatial power variation at τ_{peak} clearly indicates the location of P4. The observations show that the power flows of radio wave propagation at P3, P4, P6 are in a decreasing order.

Comparing Figure 9 (e) where Y and E stand/move at P5 and P4 respectively, to Figure 8 (a) where only E stands and moves at P4, the power variation $\Delta P_{MUS}(\phi_R, \phi_T, \tau_{peak})|_t^{t+t_{it}}$ of the former is about 1.7 dB less than that of the latter; it indicates that the movement of human at P5 does influence the whole spatial power, and decreases the power flow associated with P4. It is still difficult to differentiate the P4 and P5 locations just from the PADP variations.

(a)

(b)

(c)

(d)

(e)

FIGURE 9. PADP variations when Y and E stand at (a) P1 and P4 (b) P2 and P4 (c) P3 and P4 (d) P6 and P4 (e) P5 and P4, respectively, with FO and that when FP; the red pentagram indicates P4, the white cross indicates P1, the green dot indicates P2, the black triangle indicates P3, the magenta diamond indicates P6, and the brown triangle with green outline indicates P5.

3) THREE HUMANS

Figure 10 shows examples of the PADP variations of measured channels when three humans move from FP to FO (or the other way around) at the adjacent observation time. Figure 10 (a) shows the results when the Y, E, F stand at P6, P5, P1, respectively, that are close to Tx side, while Figure 10 (b) shows the results when they stand at P3, P4, P2, respectively, that are close to

(a)

(b)

(c)

(d)

FIGURE 10. PADP variations when Y, E, F stand at (a) P6, P5, P1 (b) P3, P4, P2 (c) P5, P1, P2 (d) P1, P5, P4, respectively, with FO and that when FP; the red pentagram indicates P4, the white cross indicates P1, the green dot indicates P2, the black triangle with red outline indicates P3, the magenta diamond indicates P6, and the brown triangle indicates P5.

Rx side. For both cases, $\Delta P_{\text{MUS}}\left(\phi_{\text{R}}, \phi_{\text{T}}, \tau_{\text{peak}}\right)|_t^{t+t_{\text{it}}}$ and $\Delta P_{\text{MUS}}\left(\phi_{\text{R}}, \phi_{\text{T}}, \tau_{\text{peak}+1}\right)|_t^{t+t_{\text{it}}}$ are able to be clearly linked to the humans' locations. In Figure 10 (a), at the peak delay bin, the variations on spatial power spectrum result in three peaks; the peaks associated to P5 and P3 are obvious while the peak associated to P1 is bit weak. At $\tau_{\text{peak}+1}$, the variations on spatial power spectrum clearly indicates the location of P1, and it suggests that the move of the human standing at P1 mainly causes changes to multiple reflections/scatterings with longer propagation path.

In Figure 10 (b), at the peak delay bin, the variations on spatial power spectrum result in two obvious peaks associated to P4 and P2. At $\tau_{\text{peak}+1}$, the variations on spatial power spectrum clearly indicates the location of P3. It is interesting since Y locates at P3 that is inside the Fresnel zone, but the move of Y does not bring obvious power variation at the peak delay bin as what E did in Figure 8 (c). It is probably due to the body figure differences, e.g. shoulder width, noting that Y is a female and is smaller than that of E who is a male.

In Figure 10 (c) where E stands at P1 and (d) where Y stands at P1, both cases can indicate the location of P1 at $\tau_{\text{peak+1}}$. At the peak delay bin, only P4 where F stands at can be suggested by observing the variations on power angular profiles $\Delta P_{\text{MUS}}\left(\phi_{\text{R}}, \phi_{\text{T}}, \tau_{\text{peak}}\right)\mid_t^{t+t_{\text{it}}}$; nevertheless, the moves of those three humans cause clear variation inside the 1st Fresnel zone, which could be due to the multiple reflections/scattering via humans then the objects inside the zone (tables/side walls) before arriving at Rx.

4) FOUR HUMANS

Examples of variations on PADP when four humans move are omitted for the sake of conciseness. Similar observations are made as in the examples shown in Figure 8, Figure 9, and Figure 10.

For the case when single human stands at one location and conducts rotational movement (to face different direction), it is rather easy to associate the peak of the variation on power angular profile at the peak delay bin of estimated PADP spectrum, i.e. $\Delta P_{\text{MUS}}\left(\phi_{\text{R}}, \phi_{\text{T}}, \tau_{\text{peak}}\right)\mid_t^{t+t_{\text{it}}}$ to the location of moving human. When more than one human stand and move, such as 2, 3, 4 humans in our measurement settings, it is rather difficult to directly associate the peaks of the variations on power angular profile to the locations of humans. The challenges lie in the following facts observed from measured data:

1) the obvious power variations may not only occur in the vicinity of different humans, but also occur in the vicinity of other background objects that interact with radio waves propagated via humans;

2) the peaks of the observable power angular spectrum variations may not equal in number with the presenting moving humans, where the number of the peaks in angular power variations may be larger than the number of humans as stated in 1), and may also be smaller than the number of humans due to the power flow at certain human location is too small to appear.

V. CONCLUSION

This paper has explored the feasibility of detecting and localizing multiple humans by using the indoor MIMO radio channel properties, namely, the power delay profile, the reverberation time, and the power angular delay profiles. In this study, the MIMO system has a bandwidth of 80 MHz, and was implemented with eight patch antennas organized in a planar configuration at link ends. To exploit the spatial domain information from the measured channels with different humans standing and moving, the super resolution algorithm of modified MUSIC with modified smoothing pre-processing is applied. The frequency samples are smoothed out for the observation in spatial domain. From the observations on the change of the reverberation time and the power angular delay profile when different humans stand and move at different locations in a meeting room, the feasibility of using reverberation time and power delay profile for detecting multiple humans, and the feasibility of using the power angular profiles at the peak and its adjacent delay bins for localizing multiple humans, are assessed.

The considered environment is considered partially reverberant. We analyzed the reverberation time, i.e. the decay rate of the slope of the power delay profile, when humans were present in the partially reverberant region. We find that both the number of humans and the direction of humans influence the reverberation time. From the measured data, one human in the partial reverberant region leads to a decrease in reverberation time of approximately 6 ns to 6.6 ns, whereas two humans yield a 12.2 ns to 15.9 ns decrease. In addition, when more than one human presents in the partial reverberant region, the turning movement of the humans results at most 4 ns change in reverberation time. These values are site-specific, but are instructive for the system design and deployment for multiple-human detection purpose.

The variation on the power angular spectrum at the peak delay bin and its successive delay bin has been investigated for its potential in indicating the location of moving humans. From numerical analysis, it is observed that the location of single human can be well indicated from the peak of the variation of the power angular profiles. However, it remains challenging to use only the power angular delay profile for indicating locations of multiple humans. The obvious power variations resulting from the moves of multiple humans may occur in the very vicinity of some of those humans, but may also occur in the vicinity of background objects that is far from target humans.

As this paper is a proof-of-concept feasibility exploration, for future work, the in-depth accuracy analysis and performance evaluation in different propagation scenarios, as well as the differentiating of multiple humans when localization will be studied.

REFERENCES

[1] K. Witrisal, P. Meissner, E. Leitinger, Y. Shen, C. Gustafson, F. Tufvesson, K. Haneda, D. Dardari, A. F. Molisch, A. Conti, and M. Z. Win, "High–accuracy localization for assisted living: 5G systems will turn multipath channels from foe to friend," *IEEE Signal Process. Mag.*, vol. 33, no. 2, pp. 59–70, Mar. 2016.

[2] M. Youssef, "CoSDEO 2016 Keynote: A decade later—Challenges: Device-free passive localization for wireless environments," in *Proc. IEEE Int. Conf. Pervasive Comput. Commun. Workshops (PerCom Workshops)*, Sydney, NSW, Australia, Mar. 2016.

[3] N. Patwari and J. Wilson, "RF sensor networks for device–free localization: Measurements, models, and algorithms," *Proc. IEEE*, vol. 98, no. 11, pp. 1961–1973, Nov. 2010.

[4] J. Shen and A. F. Molisch, "Discerning direct and indirect paths: Principle and application in passive target positioning systems," in *Proc. IEEE Global Telecommun. Conf. (GLOBECOM)*, Kathmandu, Nepal, Dec. 2011.

[5] H. Yigitler, R. Jantti, O. Kaltiokallio, and N. Patwari, "Detector based radio tomographic imaging," *IEEE Trans. Mobile Comput.*, vol. 17, no. 1, pp. 58–71, Jan. 2018.

[6] J. Wilson and N. Patwari, "Radio tomographic imaging with wireless networks," *IEEE Trans. Mobile Comput.*, vol. 9, no. 5, pp. 621–632, May 2010.

[7] X. Li, S. Li, D. Zhang, J. Xiong, Y. Wang, and H. Mei, "Dynamic–MUSIC: Accurate device-free indoor localization," in *Proc. ACM Int. Joint Conf. Pervasive Ubiquitous Comput. (UbiComp)*, Heidelberg, Germany, 2016, pp. 196–207.

[8] S.-H. Fang, T.-N. Lin, and K.-C. Lee, "A novel algorithm for multipath fingerprinting in indoor WLAN environments," *IEEE Trans. Wireless Commun.*, vol. 7, no. 9, pp. 3579–3588, Sep. 2008.

[9] M. Ohtani, H. Iwai, and H. Sasaoka, "Evaluation of terminal position estimation by position fingerprinting technique using array antenna," in *Proc. Asia–Pacific Microw. Conf. (APMC)*, Seoul, South Korea, Nov. 2013.

[10] K. Konno, N. Honma, D. Sasakawa, K. Nishimori, N. Takemura, T. Mitsui, and Y. Tsunekawa, "Estimating living–body location using bistatic MIMO radar in multi–path environment," *IEICE Trans. Commun.*, vol. E98.B, no. 11, pp. 2314–2321, 2015.

[11] A. Haimovich, R. Blum, and L. Cimini, "MIMO radar with widely separated antennas," *IEEE Signal Process. Mag.*, vol. 25, no. 1, pp. 116–129, Jan. 2008.

[12] Z. Yang, Z. Zhou, and Y. Liu, "From RSSI to CSI: Indoor localization via channel response," *ACM Comput. Surv.*, vol. 46, no. 2, pp. 1–32, Nov. 2013.

[13] J. Salmi, S. Sangodoyin, and A. F. Milisch, "High resolution parameter estimation for ultra-wideband MIMO radar," in *Proc. 11th Asilomar Conf. Signals, Syst., Comput.*, Pacific Grove, CA, USA, Nov. 2010.

[14] K. Stormo, "Human fall detection using distributed monostatic UWB radars," M.S. thesis, Sci. Robot., Norwegian Univ. Sci. Technol., Trondheim, Norway, Jun. 2014.

[15] P. Setlur, G. E. Smith, F. Ahmad, and M. G. Amin, "Target localization with a single sensor via multipath exploitation," *IEEE Trans. Aerosp. Electron. Syst.*, vol. 48, no. 3, pp. 1996–2014, Jul. 2012.

[16] Q. Pu, S. Gupta, S. Gollakota, and S. Patel, "Whole-home gesture recognition using wireless signals," in *Proc. 19th Annu. Int. Conf. Mobile Comput. Netw. (MobiCom)*, Miami, FL, USA, Oct. 2013.

[17] D. Sasakawa, N. Honma, T. Nakayama, and S. Iizuka, "Human posture identification using a MIMO array," *Electronics*, vol. 7, no. 3, p. 37, Mar. 2018.

[18] D. Sasakawa, K. Konno, N. Honma, K. Nishimori, N. Takemura, T. Mitsui, and Y. Tsunekawa, "Localizing living body using bistatic MIMO radar in multi-path environment," in *Proc. 8th Eur. Conf. Antennas Propag. (EuCAP)*, The Hague, The Netherlands, Apr. 2014.

[19] F. Adib, Z. Kabelac, and D. Katabi, "Multi-person localization via RF body reflections," in *Proc. 12th USENIX Conf. Netw. Syst. Design Implement.*, Oakland, CA, USA, May 2015, pp. 279–292.

[20] F. Liang, F. Qi, Q. An, H. Lv, F. Chen, Z. Li, and J. Wang, "Detection of multiple stationary humans using UWB MIMO radar," *Sensors*, vol. 16, no. 11, p. 1922, Nov. 2016.

[21] P. Laly, D. P. Gaillot, E. P. Simon, M. Lienard, E. Tanghe, W. Joseph, and L. Martens, "Real-time MIMO channel sounder based on a highly flexible software architecture," in *Proc. Eur. Conf. Netw. Commun.*, Paris, France, Jun. 2015.

[22] M. Landmann, M. Kaske, and R. S. Thoma, "Impact of incomplete and inaccurate data models on high resolution parameter estimation in multidimensional channel sounding," *IEEE Trans. Antennas Propag.*, vol. 60, no. 2, pp. 557–573, Feb. 2012.

[23] G. Steinbock, T. Pedersen, B. H. Fleury, W. Wang, and R. Raulefs, "Experimental validation of the reverberation effect in room electromagnetics," *IEEE Trans. Antennas Propag.*, vol. 63, no. 5, pp. 2041–2053, May 2015.

[24] J. Andersen, J. Nielsen, G. Pedersen, G. Bauch, and J. Herdin, "Room electromagnetics," *IEEE Antennas Propag. Mag.*, vol. 49, no. 2, pp. 27–33, Apr. 2007.

[25] A. Bharti, R. Adeogun, and T. Pedersen, "Estimator for stochastic channel model without multipath extraction using temporal moments," in *Proc. IEEE 20th Int. Workshop Signal Process. Adv. Wireless Commun. (SPAWC)*, Cannes, France, Jul. 2019.

[26] A. Bharti, R. Adeogun, and T. Pedersen, "Parameter estimation for stochastic channel models using temporal moments," in *Proc. IEEE Int. Symp. Antennas Propag. USNC-URSI Radio Sci. Meeting*, Atlanta, GA, USA, Jul. 2019.

[27] A. Bamba, W. Joseph, J. B. Andersen, E. Tanghe, G. Vermeeren, D. Plets, J. Ø. Nielsen, and L. Martens, "Experimental assessment of specific absorption rate using room electromagnetics," *IEEE Trans. Electromagn. Compat.*, vol. 54, no. 4, pp. 747–757, Aug. 2012.

[28] Y. Miao, T. Pedersen, M. Gan, E. Vinogradov, and C. Oestges, "Reverberant room-to-room radio channel prediction by using rays and graphs," *IEEE Trans. Antennas Propag.*, vol. 67, no. 1, pp. 484–494, Jan. 2019.

[29] W. C. Sabine, *Collected Papers on Acoustics*. Cambridge, U.K.: Harvard Univ. Press, 1922.

[30] C. F. Eyring, "Reverberation time in 'dead' rooms," *J. Acoust. Soc. Amer.*, vol. 1, no. 168, Jan. 1930.

[31] T. Pedersen, "Stochastic multipath model for the in-room radio channel based on room electromagnetics," *IEEE Trans. Antennas Propag.*, vol. 67, no. 4, pp. 2591–2603, Apr. 2019.

[32] A. Bamba, W. Joseph, G. Vermeeren, A. Thielens, E. Tanghe, and L. Martens, "A formula for human average whole-body SARwbunder diffuse fields exposure in the GHz region," *Phys. Med. Biol.*, vol. 59, no. 23, pp. 7435–7456, Dec. 2014.

[33] K. Sakaguchi, J. Takada, and K. Araki, "On measuring the delay profile and the direction of arrival by using super resolution algorithm," in *Proc. IEEE Veh. Technol. Conf.*, Ottawa, ON, Canada, May 1998, pp. 154–158.

[34] H. Yamada, M. Ohmiya, Y. Ogawa, and K. Itoh, "Superresolution techniques for time-domain measurements with a network analyzer," *IEEE Trans. Antennas Propag.*, vol. 39, no. 2, pp. 177–183, Feb. 1991.

[35] S. Pillai and B. Kwon, "Forward/backward spatial smoothing techniques for coherent signal identification," *IEEE Trans. Acoust., Speech, Signal Process.*, vol. 37, no. 1, pp. 8–15, Jan. 1989.

[36] M. Kotaru, K. Joshi, D. Bharadia, and S. Katti, "SpotFi: Decimeter level localization using WiFi," *ACM SIGCOMM Comput. Commun. Rev.*, vol. 45, no. 4, pp. 269–282, Oct. 2015.

[37] R. Schmidt, "Multiple emitter location and signal parameter estimation," *IEEE Trans. Antennas Propag.*, vol. AP-34, no. 3, pp. 276–280, Mar. 1986.

[38] V. Kristem, S. Sangodoyin, C. U. Bas, M. Kaske, J. Lee, C. Schneider, G. Sommerkorn, C. J. Zhang, R. S. Thoma, and A. F. Molisch, "3D MIMO outdoor-to-indoor propagation channel measurement," *IEEE Trans. Wireless Commun.*, vol. 16, no. 7, pp. 4600–4613, Jul. 2017.

YANG MIAO received the M.Sc. and Ph.D. degrees from the Antenna and Radio Propagation Laboratory, Department of International Development Engineering, Tokyo Institute of Technology, Tokyo, Japan, in 2012 and 2015, respectively.

From 2010 to 2015, she was a Research Assistant with the Takada Laboratory, Mobile Communications Research Group, Tokyo Institute of Technology. From 2015 to 2018, she was a Postdoctoral Researcher with the Institute of Information and Communication Technologies, Electronics, and Applied Mathematics, Universite Catholique de Louvain, Louvain-la-Neuve, Belgium, and IMEC, Wireless, Acoustics, Environment, and the Expert Systems Laboratory, Ghent University, Ghent, Belgium. From 2017 to 2018, she was a part-time Senior Antenna Engineer with Jaguar Radio Wave Corporation, Shenzhen, China. Since 2018, she has been a Research Assistant Professor with the Southern University of Science and Technology, Shenzhen, China. She has been an Assistant Professor with the Telecommunication Engineering Group, University of Twente, The Netherlands, since autumn 2019. Her current research interests include interactions between antenna arrays and physical radio propagation environment, both in physical layer and system level, radio channel measurement, modeling, and characterization, multiantenna array configuration and massive MIMO topology, reverberation and room electromagnetics, applications of radio channel in human detection and posture identification, in over-the-air testing of wireless devices, and in critical propagation environment, such as unmanned aerial vehicle communications.

EMMERIC TANGHE was born in Tielt, Belgium, in August 1982. He received the M.Sc. degree in electrical engineering and the Ph.D. degree in electrical engineering from Ghent University, Ghent, Belgium, in 2005 and 2011, respectively. From September 2005 until May 2011, he was a Research Assistant with the Department of Information Technology, Ghent University (imec-UGent/INTEC). His scientific work focused on the modeling of indoor and outdoor propagation through field measurements. Since May 2011, he has been a Postdoctoral Researcher with the Ghent University, where he is involving in propagation modeling. From October 2012 until September 2018, he was a Postdoctoral Fellow of the FWO-V (Research Foundation–Flanders). In October 2015, he became a part-time Professor in medical applications of electromagnetic fields in and around the human body.

JUN-ICHI TAKADA (Senior Member, IEEE) received the Ph.D. degree in electrical and electronic engineering from the Tokyo Institute of Technology (Tokyo Tech), in 1992. After served as a Research Associate with Chiba University, from 1992 to 1994, and as an Associate Professor with Tokyo Tech, from 1994 to 2006, he has been a Professor with Tokyo Tech, since 2006, where he is currently serving as the Vice Chair of the Department of Transdisciplinary Science and Engineering, School of Environment and Society. From 2003 to 2007, he was a Researcher with the National Institute of Information and Communication Technology, Japan. His current research interests include radio-wave propagation and channel modeling for mobile and short range wireless systems, applied measurement using radio wave, and ICT applications for international development. He is a Fellow of Information and Communication Engineering (IEICE), Japan, and a member of Japan Society for International Development.

TROELS PEDERSEN received the M.Sc. degree in digital communications and the Ph.D. degree in wireless communications from Aalborg University, Aalborg, Denmark, in 2004 and 2009, respectively.

In 2005, he was a Guest Researcher with the FTW Telecommunications Research Center Vienna, Vienna. He has been with the Department of Electronic Systems, Aalborg University, since 2009, as an Assistant Professor, and since 2012, as an Associate Professor. In 2012, he was a Visiting Professor with IETR, Rennes, France, and the University of Rennes 1, Rennes. His current research interests are within statistical signal processing and communication theory, including sensor array signal processing, radio geolocation techniques, radio channel modeling, and radio channel sounding. He received the Teacher of the Year Award twice by the Study Board for Electronics and IT, Aalborg University, in 2011 and 2017, respectively.

PIERRE LALY is currently an Engineer of study. His main current areas of research are the study, design, and production of electronic cards to build prototypes dedicated to digital and/or analog telecommunications. He realizes the implementation and programming of microcontrollers, DSP, CPLD, FPGA components, and the study and the realization of sub systems for the recovery and the statistical treatment of the information of the various prototypes. It also handles the maintenance and installation of computer equipment of TELICE.

DAVY P. GAILLOT was born in Arras, France, in October 1978. He received the B.Sc. degree in mechanical engineering from the École Nationale d'Ingénieurs de Metz (ENIM), Metz, France, in 2002, the M.Sc. degree in mechanics, materials, structures, and processes from the University of Metz, Metz, in 2002, and the Ph.D. degree in materials science and engineering from the Department of Materials Science and Engineering, Georgia Institute of Technology, Atlanta, GA, USA, in 2007. Since 2008, he has been an Associate Professor with the IEMN/TELICE Group, University of Lille 1 (Institut d'Electronique, de Microélectronique et de Nanotechnologie/Télécommunications, Interférences et Compatibilité Electromagnétique), Villeneuve d'Ascq, France. His research interest includes the development of outdoor/indoor radio channel models for localization techniques that are supported by legacy or upcoming millimeter-wave and centimeter-wave wireless network standards. In addition, he focuses on highly diffuse and industrial radio channels for propagation modeling and exposure assessment.

MARTINE LIÉNARD received the Ph.D. degree in telecommunication from the University of Lille, in 1993.

Since 1990, she has been with the Telecommunications, Interferences and Electromagnetic Compatibility (TELICE) Group, Institute of Electronic, Microelectronic and Nanotechnology (IEMN), University of Lille, where she is currently a Professor and the Head of the TELICE Group. Her current research deals with mobile localization techniques in non-cooperative mode, theoretical and experimental prediction of propagation characteristics in complex environment, MIMO and massive MIMO challenges mainly dedicated for rail, and road transportation communication systems and industry 4.0.

LUC MARTENS received the M.Sc. degree in electrical engineering from Ghent University, Belgium, in July 1986, and the Ph.D. degree, in December 1990. From September 1986 to December 1990, he was a Research Assistant with the Department of Information Technology (INTEC), Ghent University. During this period, his scientific work was focused on the physical aspects of hyperthermic cancer therapy. His research work dealt with electromagnetic and thermal modeling and with the development of measurement systems for that application. Since 1991, he has been managing the Wireless and Cable (WiCa) Research Group, INTEC. Since 2004, the WiCa Research Group has been a part of the iMinds Institute and since April 1993, he has been a Professor with Ghent University. His experience and current interests are in modeling and measurement of electromagnetic channels, of electromagnetic exposure, e.g., around telecommunication networks and systems, such as cellular base station antennas, and of energy consumption in wireless networks. He is author or coauthor of more than 300 publications in the domain of electromagnetic channel predictions, dosimetry, exposure systems, and health and wireless communications.

WOUT JOSEPH (Member, IEEE) was born in Ostend, Belgium, in October 1977. He received the M.Sc. degree in electrical engineering from Ghent University, Belgium, in July 2000, and the Ph.D. degree, in March 2005. From September 2000 to March 2005, he was a Research Assistant with the Department of Information Technology (INTEC), Ghent University. During this period, his research work dealt with measuring and modeling of electromagnetic fields around base stations for mobile communications related to the health effects of the exposure to electromagnetic radiation. From April 2005 to April 2009, he was Postdoctoral Researcher for iMinds-UGent/INTEC. From October 2007 to October 2013, he was a Postdoctoral Fellow of the FWO-V (Research Foundation–Flanders). Since October 2009, he has been a Professor with the domain of Experimental Characterization of wireless communication systems. He is has also been with IMEC PI, since 2017. He is author of more than 500 publications. His professional interests are electromagnetic field exposure assessment, in-body electromagnetic field modeling, electromagnetic medical applications, propagation for wireless communication systems, the IoT, antennas, and calibration.

• • •